Emissivity modeling of thermal radiation sources with concentric grooves

Alexander V Prokhorov, Sergey N Mekhontsev, Leonard M Hanssen
Optical Technology Division, National Institute of Standards and Technology, 100 Bureau Drive, Gaithersburg, MD 20899-8441, USA; fax: +1 301 840 8551; email: leonard.hanssen@nist.gov
Presented at the 16th European Conference on Thermophysical Properties, Imperial College, London, England, 1 – 4 September 2002

Abstract. Monte-Carlo-based specialized software has been applied to the statistical modeling of effective emissivity of radiators with concentric grooves of trapezoidal and triangular profile. A specular-diffuse model is used in which the thermal emission from the walls obeys Lambert's cosine law, and reflection may have both specular and diffuse (Lambertian) components. The angular dependences of effective emissivity of a radiator with concentric triangular and trapezoidal grooves are computed for various values of the diffuse component. Grooves with isothermal and non-isothermal walls are modeled. It is shown that a temperature drop towards the peak of a groove might lead to substantially decreased effective emissivity. An example of a modeling result for a grooved radiator with reflector enhancement is presented.

1 Introduction

Use of parallel rectilinear or annular concentric grooves is a well-known approach to increase the emissivity of compact blackbody radiators, improve the absorptance of stray radiation traps, baffles, and thermal radiation detectors, as well as enhance thermal radiation transfer. Emitters with grooved surfaces are widely used as reference sources in radiation thermometry and radiometry (Johnson et al 1995; Hoogeveen et al 1998). In the design phase of such devices it is important to be able to predict their performance.

Numerous papers are devoted to the modeling of a rectilinear groove with purely diffuse or purely specular reflectance. Daws (1954) examined the angular emission properties for a rectilinear groove with an isosceles triangular profile and isothermal diffuse walls on the basis of approximate expressions for directional and hemispherical effective emissivity. Sparrow and Gregg (1962) published numerical solutions of Fredholm's integral equations of the 2nd kind, which describe the radiation heat exchange in an infinite groove with a rectangular profile. Sparrow and Lin (1962) considered the absorption of thermal radiation in a triangular groove with purely diffuse or purely specular walls. Their results could be applied to an emitting groove by use of the reciprocity principle and Kirchhoff's law. Psarouthakis (1963) derived the simple but powerful analytical formula for effective emissivity of an isothermal diffuse triangular groove. O'Brien and Heckert (1965) obtained an exact solution for the effective emissivities of isothermal and non-isothermal specular grooves with a triangular shape. They also found an approximate numerical solution for both isothermal and non-isothermal diffuse grooves. Zhimin (1987) proposed an approximate solution of an integral equation describing radiative heat transfer in both isothermal and non-isothermal diffuse rectilinear grooves with a triangular shape and obtained the dependence of total directional, normal, and hemispherical emissivities on several critical parameters. We are not aware of any papers that have addressed the modeling of concentric grooves for enhanced emissivity.

Radiation properties of annular concentric grooves differ from those associated with rectilinear parallel grooves (eg when comparing ray trajectories at oblique viewing of rectilinear and annular grooves of triangle section with specularly reflecting walls),

and become similar only at large values of the ratio of the radial coordinate to the groove period, where the curvature of the annular grooves tends to zero. We intend to address the lack of modeling with a study of isothermal and non-isothermal concentric grooves with mixed specular-diffuse reflection for various viewing conditions.

2 Computational model and method

Our analysis has been performed by application of the STEEP3 [1] code to numerical modeling of grooved surfaces. This code, which employs the Monte-Carlo method, is described by Sapritsky and Prokhorov (1992, 1995), and Prokhorov and Martin (1996). It is used to compute the spectral and total effective emissivity of enclosures formed by rotation of non-self-crossing polygonal lines around any axis. Each surface can have arbitrary distributions of temperature and specular-diffuse reflectance.

According to the specular-diffuse model, we specify radiation properties by a directional-hemispherical reflectance $\rho = 1 - \varepsilon$, where ε is the hemispherical emissivity, and a diffusity (not to be confused with diffusivity) D defined as the ratio of the diffuse component of reflectance to the total reflectance. Diffusity can be an arbitrary function of incident angle, but the inequality $0 \leqslant D \leqslant 1$ must be obeyed, and ρ must be independent of incident angle. Unless stated otherwise, we will deal with spectral quantities.

The specular-diffuse model is a crude but useful approximation of the reflection properties of real materials and coatings. In most cases, specular reflection becomes dominant for large incident angles. One can simulate this effect by prescribing to the diffusity D a function that decreases with increasing incidence angle. In addition, the directional-hemispherical reflectance of real-world materials tends to increase with increasing incidence angle. However, we have limited the scope of our study by the bounds of the specular-diffuse model. More complex modeling as well as more experimental goniophotometric data are required for exact solutions that take account of the real angular distributions of reflected fluxes.

The *spectral local directional effective emissivity* is defined as the ratio of the spectral radiance for a given location, wavelength, temperature, and direction to the spectral radiance of a perfect blackbody for the same wavelength, temperature, and direction. The appropriate average effective emissivities can be obtained by averaging over a spectral range, solid angle, and/or viewed area. In figure 1, the viewing conditions for the three most important types of effective emissivity are depicted schematically.

The *local normal effective emissivity* corresponds to observation along a ray, which is parallel to the radiator axis. The *average normal effective emissivity* is applicable to a case when detector of radius R is coaxial with the radiator and located at an infinite distance from it. The *average directional effective emissivity* corresponds to the observation of parallel rays at an angle γ.

We study radiators with concentric grooves of trapezoidal profile (figure 2). The geometric parameters of this structure are: p is the pitch (or period), f_t and f_b are the widths of the flat areas at the top and bottom, and β is the angle between lateral sides of the trapezoid. The groove shape becomes triangular if $f_t = f_b = 0$. We assume that the center of the radiator is always concave.

[1] Certain commercial software is identified in this paper in order to specify the computational procedure adequately. Such identification is not intended to imply recommendation or endorsement by the National Institute of Standards and Technology, nor is it intended to imply that the software identified is necessarily the best available for the purpose.
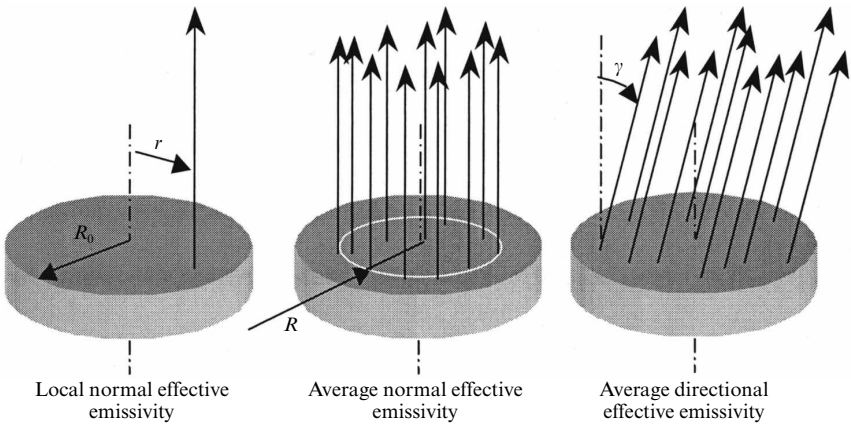
Figure 1. Viewing conditions for different types of effective emissivity.
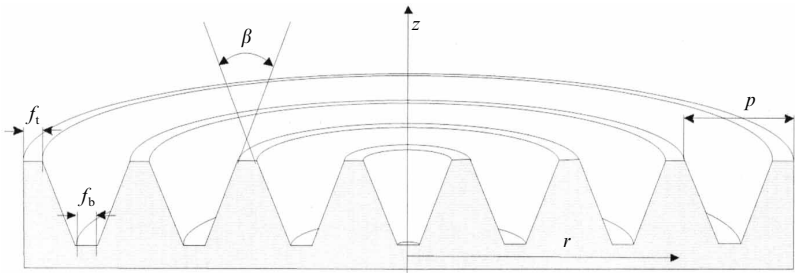
Figure 2. Geometrical model of the radiator: p is the pitch, f_t and f_b are the widths of the flat areas at the top and bottom, and β is the included angle.

3 Isothermal concentric triangular grooves

### 3.1 *Local and average effective emissivity of diffuse grooves*

Figure 3 shows the calculated distribution of the local effective emissivity for isothermal diffuse triangular grooves as a function of the dimensionless radial coordinate for triangular grooves with unit period and three values of the angle β at the groove vertices. The local effective emissivity reaches a maximum at the groove bottoms and monotonically decreases towards the groove peaks. The use of a radiometer with a finite field of view (FOV) to scan the radiator along its diameter would flatten these oscillations.

For figures 4–7, we use a radiator with a radius $R_0 = 50$ relative linear units, $p = 1$, and the depth of grooves determined by the angle at their apices. In figure 4, the normal effective emissivity of an isothermal diffuse radiator with triangular concentric grooves is shown as a function of the visible area radius for three values of the angle β and for a surface emissivity ε of 0.7. The normal effective emissivity (averaged over viewing area) changes by the law of damped oscillations with increasing viewing area. The effect can be explained by the alternation of peak-adjacent and valley-adjacent regions of the groove as a boundary of the viewing area. In the limiting case of infinitely large viewing radius (and, therefore, zero curvature of surfaces forming the groove), it asymptotically approaches the effective emissivity of linear parallel grooves.

The dependences depicted in figures 3 and 4 show that viewing a small number of concentric grooves may lead to poor repeatability of measurements due to inaccuracy of sighting.
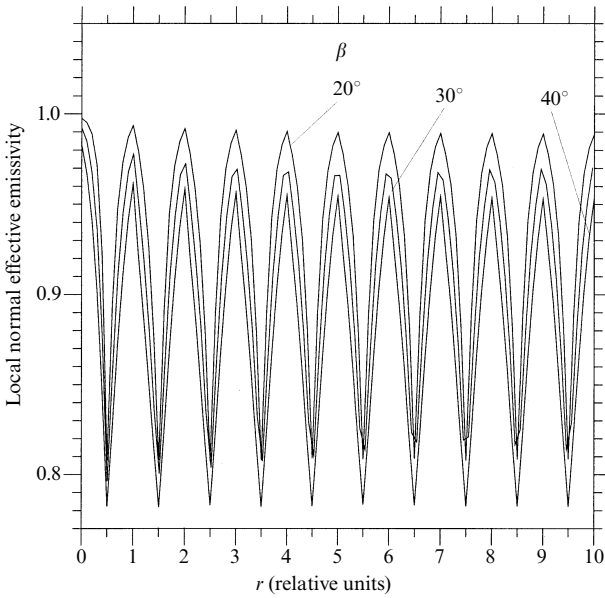
Figure 3. Local effective emissivity for three values of the angle β ($20°$, $30°$, and $40°$); $p = 1$, $\varepsilon = 0.7$, and $D = 1$.
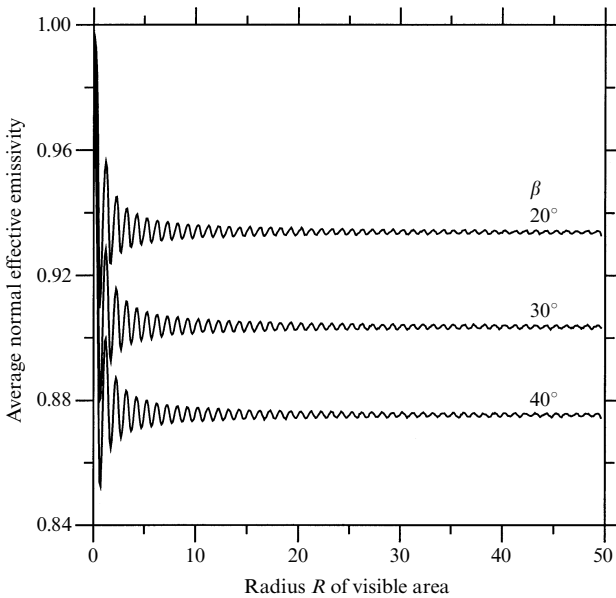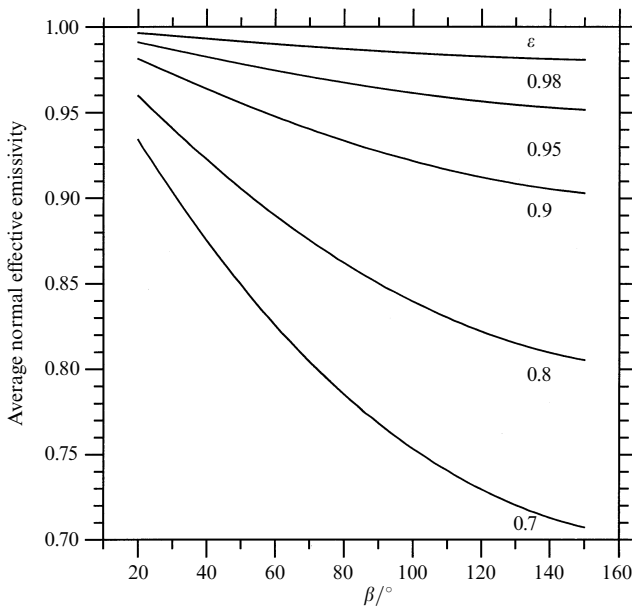

Figure 4. Average normal effective emissivity as a function of the visible area of radius R for three values of the angle β ($20°$, $30°$, and $40°$) at the vertex of triangular grooves; $p = 1$, $\varepsilon = 0.7$.

3.2 *Normal average emissivity as a function of groove apex angle and diffusity*

We performed numerical experiments to investigate the interrelationships between the wall emissivity, diffusity, groove apex angle, and normal effective emissivity. For all plots in figures 5 – 7, $p = 1$, the entire radiator is viewable, and $R = R_0 = 50$.

Curves in figure 5 show the dependence of the normal effective emissivity on the angle β at the vertex of the diffuse ($D \equiv 1$) triangular grooves for surface emissivity of 0.7, 0.8, 0.9, 0.95, and 0.98.
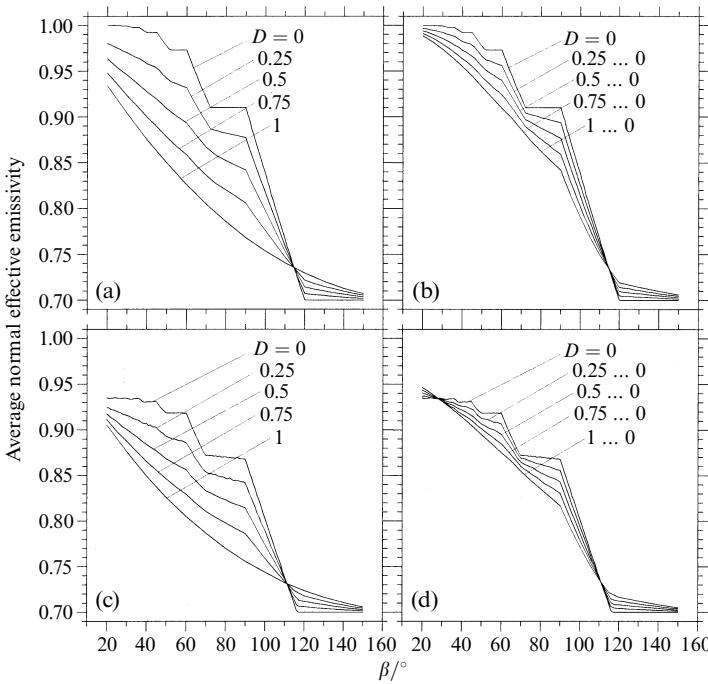
Figure 5. Average normal effective emissivity as a function of the angle β at the vertex of diffuse triangular grooves for five values of surface emissivity ε (0.7, 0.8, 0.9, 0.95, and 0.98), and $R = R_0 = 50$.

Figure 6 illustrates the effects of the introduction of a specular component into the reflectance for a groove wall emissivity $\varepsilon = 0.7$ and several values of diffusity D at normal incidence. The curves in figures 6a and 6b refer to triangular grooves ($f_t = f_b = 0$), and in figures 6c and 6d to trapezoidal grooves ($f_t = f_b = 0.1$). Curves are shown for constant (independent of incidence angle) values of the diffusity D of groove walls in figures 6a and 6c. Curves for varying diffusity D ranging from maximum values of 0, 0.25, 0.5, 0.75, and 1, respectively, for normal incidence, and linearly decreasing to 0 for $90°$ incidence are shown in figures 6b and 6d.

In figures 6a and 6c, for purely specular reflection, the dependence of normal effective emissivity on the angle β is stepped owing to the step change in the number of reflections. The presence of a diffuse component leads to a decrease in the effective emissivity for β less than about 115°. For β greater than this value, the inversion of curve order is observed. In the case of trapezoidal grooves with $f_t = f_b = 0.1$ (see figure 6c), the normal effective emissivity for each angle and coating has a lower value compared to the triangular case (owing to the lower values of local emissivities of flat areas).

The introduction of a linear dependence of the diffusity on incidence angle in figures 6b and 6d shifts all curves toward the curve representing perfect specular reflection ($D = 0$). At normal incidence, the curves remain stepped even for values of diffusity close to 1. This result can be explained in the following manner. Through general considerations, numerically proven by Prokhorov et al (2003), if reflection from surfaces of radiator obeys the reciprocity principle, we can reverse ray paths to trace rays from a viewing point to the radiator. This algorithm, known as 'backward ray tracing', is employed in the software used for the current study. For rays that propagate parallel to the radiator axis, the first angle of incidence onto a wall of a groove with apex angle β is equal to $\frac{1}{2}(\pi - \beta)$. The smaller the angle at the groove apex, the closer the incidence angle is to $\frac{1}{2}\pi$, and hence the smaller the diffusity. For surfaces with high emissivity, the first reflection is determinative. Thus, the major portion of radiant flux is reflected specularly. This makes the behavior of the curves for $D \neq 0$ in figures 6b and 6d similar to that for purely specular reflection.

Figure 6. Normal effective emissivity of isothermal grooves vs angle β: (a) and (b), triangular grooves ($f_t = f_b = 0$); (c) and (d), trapezoidal grooves ($f_t = f_b = 0.1$). In (a) and (c), diffusity D of groove walls is independent of incidence angle; in (b) and (d), diffusity D ranges from the values of 0, 0.25, 0.5, 0.75, 1, respectively, for normal incidence and linearly decreases down to 0 for the incidence angle of 90°. For all cases $\varepsilon = 0.7$; $R = R_0 = 50$.

For real-world surfaces, the growth of effective emissivity with decreasing groove apex angle is limited by the increase of the directional-hemispherical reflectance for grazing incidence. Moreover, a specular lobe rather than a sharp specular ray is often observed. But, as mentioned above, such a more realistic model of reflection is out of the scope of the specular-diffuse model used in this work. For the remainder of our studies we will assume that the diffusity D is independent of incidence angle.
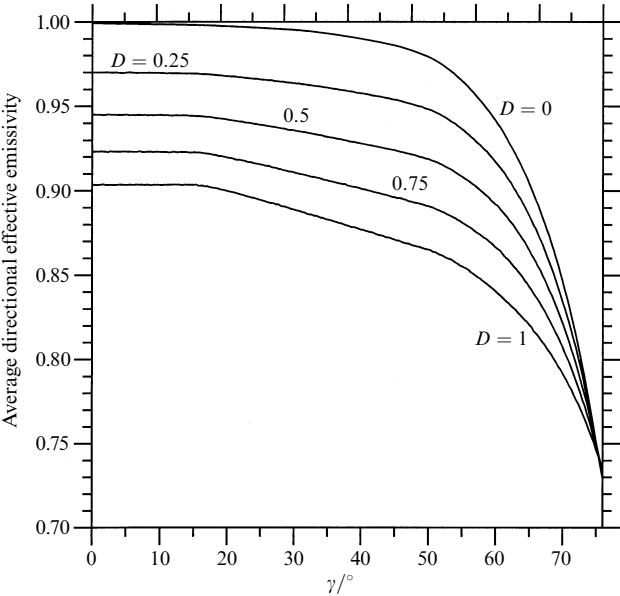
3.3 Directional effective emissivity

The angular properties of radiators with concentric triangular grooves have been studied. The computed dependence of the average directional emissivity for isothermal 30° triangular grooves with wall emissivity 0.7 are depicted in figure 7. For values of diffusity $D = 0$ to 1, the effective emissivity decreases with increasing viewing angle γ, ie the angle with respect to the normal to the flat surface of the radiator (prior to groove machining). All curves have a salient point (abrupt change of curvature) when $\gamma = \frac{1}{2}\beta$. For the groove geometry considered, this corresponds to the onset of the 'masking effect' when the observer ceases to register radiation from one of the groove walls.

4 Non-isothermal concentric grooves

In real radiators, the heat loss due to radiation from the groove walls leads to a temperature gradient along the groove depth. In the case where the temperature of the environment is lower than that of the radiator, peaks will be colder than valleys.

For modeling, we have chosen the temperature of the groove bottoms as the reference temperature (ie the temperature at which Planck's function is computed) and linearly interpolated temperatures between the groove bottom and top.

Figure 7. Dependence of the directional effective emissivity of isothermal 30° triangular grooves on the angle of view, γ, for several values of diffusity D; $R = R_0 = 50$.
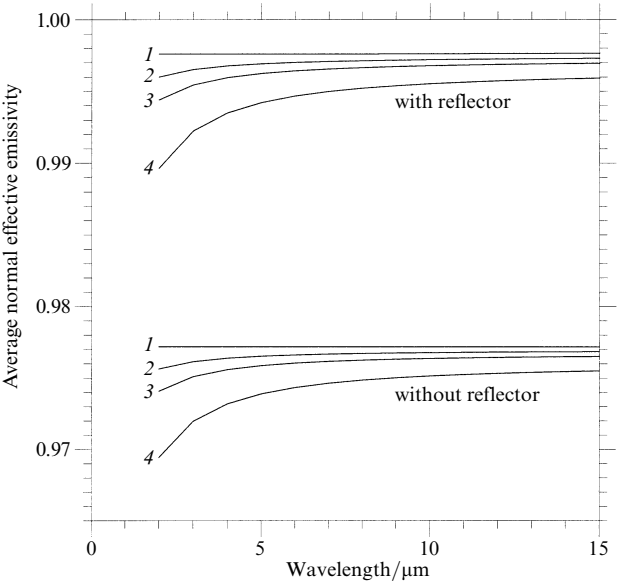
Figure 8. The normal effective emissivity of trapezoidal grooves with diffuse gray walls, with and without reflector, for four values of linear temperature decrease (1—0 K, 2—0.5 K, 3—1 K, 4—2.5 K) toward the groove vertices.

The spectral normal effective emissivities of a radiator with trapezoidal grooves ($p = 4$, $f_t = 0.2$, $f_b = 1$, $\beta = 38.58°$) with diffuse gray walls (emissivity 0.95) and for several values of temperature decrease towards the groove vertices (0 K, 0.5 K, 1 K, and 2.5 K) are depicted in the lower part of figure 8. The temperature at the groove valley is 1000 K. The results obtained show that the temperature gradient along the groove walls leads to a significant decrease of the spectral effective emissivity, especially in the short-wave spectral range.

5 Blackbody radiator with grooved bottom

Often grooved bottoms are used in the construction of cavity radiators. The placement of a grooved radiator into an enclosure reduces the radiation and convection heat losses and, therefore, flattens the temperature field of the grooves.

We considered an example of a blackbody calibration radiator that consists of a grooved bottom with the same parameters as in the example of the previous section, and a reflector with a specialized profile (figure 9) as described by Mekhontsev et al (1998) and Sapritsky et al (1998). We assumed that the profiled reflector is purely specular with an emissivity of 0.015. Its temperature changes linearly from 400 K near the bottom to 300 K near the aperture. As one can see in figure 8, the placement of a grooved bottom under the profiled reflectors substantially increases its emissivity. With the growth of a temperature difference between the tops and bottoms of the grooves, the spectral effective emissivity decreases, repeating the behavior of the appropriate curves in the lower part of the figure.
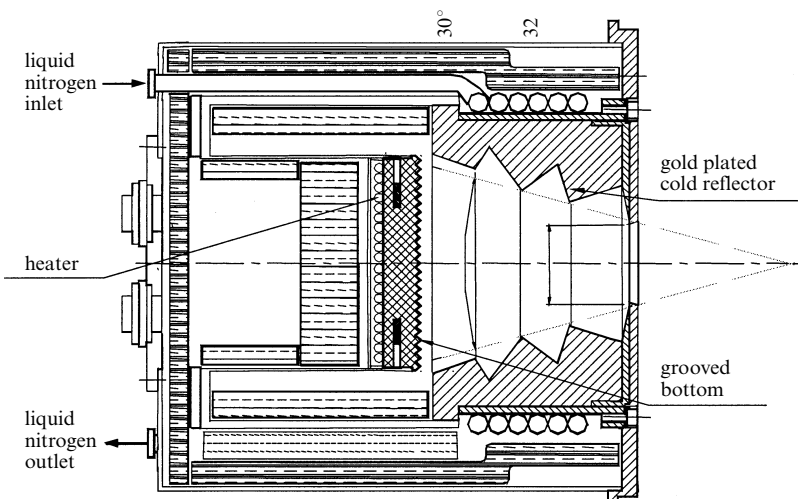

Figure 9. A sectional view of the blackbody calibration source BB1000.

6 Conclusions

An analysis of the results of the numerical experiments suggests the following:

(a) effective emissivity modeling for concentric non-isothermal grooved radiators with specular-diffuse coatings can be performed, allowing selection of appropriate geometry and coatings to maximize average effective emissivity and/or local directional radiance uniformity for given constraints (such as overall dimensions);

(b) uncertainty evaluations of the effects of variations in coating properties, temperature gradients and manufacturing artifacts (such as surface irregularity), as well as alignment of the FOV, can be undertaken;

(c) the results obtained can be helpful to a user to predict the performance of specular/diffuse surfaces with concentric grooves, as well as understand experimental results.

Further improvement of the model can be achieved by performing finite-element analysis for estimates of the temperature gradients, including background radiation effects, as well as by introducing a more realistic reflectance model.

References

Daws L F, 1954 *Brit. J. Appl. Phys.* **5** 182 – 187
Johnson D G, Jucks K W, Traub W A, Chance K V, 1995 *J. Geophys. Res.* **100** 3091 – 3106

Hoogeveen R W M, Bernard C, Helmich F P, de Jonge A R W, Wijnbergen J J, Goede A P H, 1998 *32nd ESLAB Symposium: Remote Sensing Methodology for Earth Observation and Planetary Exploration, 15 – 18 September 1998 at ESTEC, Noordwijk, The Netherlands* pp 139 – 146

Mekhontsev S N, Sapritsky V I, Prokhorov A V, Khromchenko V B, Samoilov M L, 1998 *Proc. SPIE* **3553** 247 – 258

O'Brien P F, Heckert B J, 1965 *Illum. Eng.* **4** 187 – 195

Prokhorov A V, Martin J E, 1996 *Proc. SPIE* **2815** 160 – 168

Prokhorov A V, Hanssen L M, Mekhontsev S N, 2003, in *Proceedings of the 8th International Temperature Symposium, 21 – 24 October 2002, Chicago, IL* volume 7, pp 729 – 734

Psarouthakis J, 1963 *J. Am. Inst. Aeron. Astron.* **1** 1879 – 1882

Sapritsky V I, Mekhontsev S N, Prokhorov A V, Sudarev K A, Khromchenko V B, Samoilov M L, 1998 *Proc. SPIE* **3437** 434 – 445

Sapritsky V I, Prokhorov A V, 1992 *Metrologia* **29** 9 – 14

Sapritsky V I, Prokhorov A V, 1995 *Appl. Opt.* **34** 5645 – 5652

Sparrow E M, Gregg J L, 1962 *J. Heat Transf.* C **84** 270 – 271

Sparrow E M, Lin S H, 1962 *Int. J. Heat Mass Transf.* **5** 1111 – 1115

Virial Inc., 2000 *STEEP3 v. 1.3, Blackbody Emissivity Modeling Program: User's Guide* (New York: Virial Inc.)

Zipin R B, 1966 *J. Res. Natl. Bur. Stand.* C **70** 275 – 280

Zhimin Z, 1987 *Proc. SPIE* **810** 270 – 277

p